16 Combined TDR and Low-Frequency Permittivity Measurements for Continuous Snow Wetness and Snow Density Determination

Markus Stacheder[1], Christof Huebner[2], Stefan Schlaeger[3], Alexander Brandelik[1]

[1]Research Center Karlsruhe, Institute of Meteorology and Climate Research
[2]Fachhochschule Mannheim – University of Applied Sciences
[3]Research Center Karlsruhe, Institute of Technical Chemistry

16.1 Introduction

Measuring snow wetness and density is essential for many applications in snow hydrology like avalanche warning, flood prediction, optimization of hydro power generation, and investigations of glacier melting due to global warming and climate change. Seasonal snow cover is highly variable in both space and time, especially when melting occurs. Deposition and depletion represents sporadic rather than continuous processes varying with meteorological conditions. After initial deposition, snow layers change over time and display a wide range of physical characteristics, from metamorphism of snow crystals and grains to melting processes and liquid water transport. The vertical arrangement of different snow layers and their properties is most important for avalanche prediction. The total snow water equivalent represents the available supply for filling the reservoirs of hydro power stations. Monitoring the variations of temporal snow wetness is essential for determining water percolation through the snow pack and the assessment of flood danger. Therefore several measurement stations at representative sites within a hydrological basin or area of interest are required. The sensors themselves have to provide vertically resolved mean snow properties of a sufficiently large area at these sites.

So far snow sensors are not suitable for long-term continuous measurements when disturbing melting processes occur around the sensor, nor are they capable of measuring snow wetness and density at the same time with sufficient accuracy. The performance of these sensors, moreover, suffers from their small measurement volume which is not adequate to achieve representative values for natural snow cover with its large spatial variability. These sensors usually consist of coaxial lines, two-wire lines, microstrip lines, or capacitor plates (Fig. 16.1). They measure the permittivity of the snow in their surroundings from which the water content and/or the density of the snow can be derived.

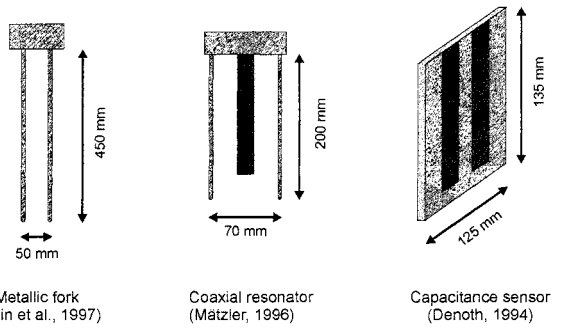

Fig. 16.1. Conventional snow moisture sensors [1], [2], [3]

One of these sensors has been used during a measurement campaign to determine the spatial variability of wetness in natural snow cover. A trench 16 m long and about 0.5 m deep was excavated in the snow. The water content along the trench was measured with the Denothsensor [4] at two consecutive days at a depth of about 0.5 m below the surface and with 1 m spacing (Fig. 17.2).

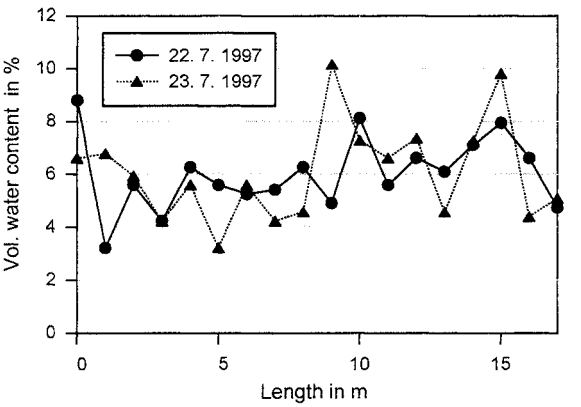

Fig. 16.2. Water content of a high Alpine snow pack at two consecutive days measured with a Denothsensor

The measurement results show strong fluctuations of water content which are typical of the time of the year with daily melting and nightly freezing. When water flow starts, rapid changes in the snow pack occur and preferential percolation paths emerge. A high temporal and spatial variability of the snow wetness is the result. Hence, on one hand, destructive methods are not practical for studying temporal evolutions. On the other hand representative mean values of snow wetness require a large number of measurements and consequently an enormous expenditure of work.

Therefore a new sensor has been developed. It consists of a flat band cable as a transmission line up to about 100 m long which is enclosed by snowfall. TDR

measurements in combination with low-frequency measurements are suitable for the determination of both snow wetness and density at the same time. Besides integral measurements along the flat band cable, the reconstruction of snow parameter profiles with a sloping configuration is possible as well.

16.2 Dielectric Properties of Snow

Dry snow is a mixture of ice crystals (volumetric fraction *I*) and air (volumetric fraction *A*). Wet snow contains an additional fraction of liquid water (*W*). The relative dielectric permittivity of ice, ε_{ice}, and water, ε_w, are frequency and temperature dependent, whereas the permittivity of air, ε_a, is equal to 1. Figure 16.3 shows the relaxation spectra for water and ice at a temperature of 0°C.

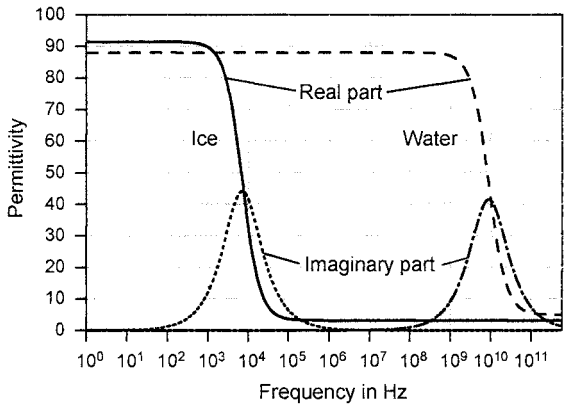

Fig. 16.3. Relaxation spectra of water and ice at a temperature of 0°C

The relaxation frequency of ice is much lower than that of water due to the strong binding forces within the ice crystal. Wet snow has a constant temperature of 0°C, whereas dry snow has varying temperatures below or equal to 0°C. Therefore only the temperature-dependent permittivity of ice has to be accounted for.

Experimental evidence indicates that the permittivity of ice may be considered independent of both temperature (below 0°C) and frequency in the microwave region and may be assigned the constant value 3.15 [5]. But at lower frequencies, e.g., in the kilohertzrange, the permittivity of ice depends considerably on temperature (Fig. 16.4).

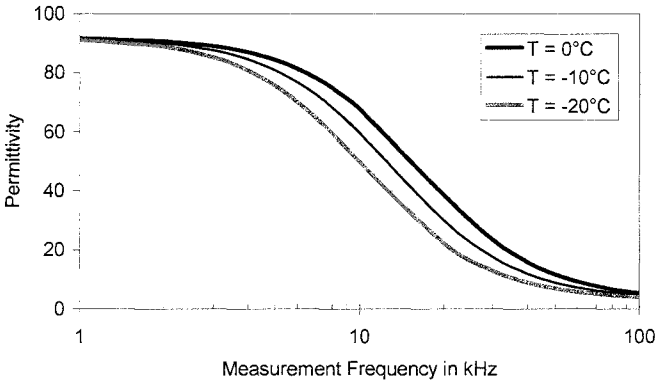

Fig. 16.4. Temperature-dependent permittivity of ice

The complex permittivity of ice, ε_{ice}, is given by

$$\varepsilon_{ice}(f,T) = \varepsilon_{\infty} + \frac{\varepsilon_{ice,static} - \varepsilon_{ice,\infty}}{1 + jf / f_{rel}(T)} \tag{16.1}$$

with temperature-dependent relaxation frequency

$$f_{rel}(T) = \frac{1}{2\pi} 10^{-\left(\frac{664.873}{T} - 7.447\right)}. \tag{16.2}$$

The static permittivity is $\varepsilon_{ice,static} = 92.0205$, whereas the high-frequency limit is $\varepsilon_{ice,\infty} = 3.16$ [5]. The permittivity of water is considered to be real and independent of frequency within the measurement range below 1 GHz:

$$\varepsilon_w(f < 10^9\, Hz, T = 0°C) = 88. \tag{16.3}$$

The permittivity of snow, ε_{snow}, is related to the volumetric fractions of the constituents ice, water, and air and their dielectric properties. This relation can be described by an adequate mixing rule. Looyenga's formulae [6] for spherical intrusions ($\alpha = 0.3$) is in close agreement with experimental results:

$$\varepsilon_{snow}(f,T) = \left(W\varepsilon_w^{\alpha} + I\varepsilon_{ice}^{\alpha}(f,T) + A\varepsilon_a^{\alpha}\right)^{1/\alpha} \tag{16.4}$$

with $W + I + A = 1$ for the unity volume.

16.3 Measurement Principle

In order to determine the two unknowns, water content and density, two independent equations are required. These are

$$\varepsilon_{snow}(f_1) = \left(W\varepsilon_w^\alpha + I\varepsilon_{ice}^\alpha(f_1,T) + A\varepsilon_a^\alpha\right)^{1/\alpha} \tag{16.5}$$

$$\varepsilon_{snow}(f_2) = \left(W\varepsilon_w^\alpha + I\varepsilon_{ice}^\alpha(f_2,T) + A\varepsilon_a^\alpha\right)^{1/\alpha} \tag{16.6}$$

with $\varepsilon_{snow}(f_1)$ and $\varepsilon_{snow}(f_2)$ as permittivity measurements at two frequencies with different water to ice permittivity ratios.

The equation set can be solved for water content, W, and ice fraction, I, using $W + I + A = 1$ as follows

$$I = \frac{\varepsilon_{snow}^\alpha(f_1) - \varepsilon_{snow}^\alpha(f_2)}{\varepsilon_{ice}^\alpha(f_1,T) - \varepsilon_{ice}^\alpha(f_2,T)} \tag{16.7}$$

$$W = \frac{\varepsilon_{snow}^\alpha(f_1) - 1 - \dfrac{\varepsilon_{snow}^\alpha(f_1) - \varepsilon_{snow}^\alpha(f_2)}{\varepsilon_{ice}^\alpha(f_1,T) - \varepsilon_{ice}^\alpha(f_2,T)}\left(\varepsilon_{ice}^\alpha(f_1,T) - 1\right)}{\varepsilon_w^\alpha - 1}. \tag{16.8}$$

The snow density, D, can be derived from water content, W, and ice fraction, I, as follows

$$D = W \cdot 0.9999 + I \cdot 0.9150 \tag{16.9}$$

taking into account the different densities of liquid water (0.9999) and ice (0.9150). In order to achieve maximum accuracy the differences between the water to ice permittivity ratio at the two frequencies should be as large as possible. This can be achieved by using a low frequency (smaller than the relaxation frequency of ice) and a high frequency (higher than the relaxation frequency of ice and lower than the relaxation frequency of water). Typical frequencies are below 10 kHz for f_1 and frequencies between 100 kHz and 1 GHz for f_2.

16.4 Flat Band Cable Sensor

Instead of the small-scale sensors (Fig. 16.1) with their rigid and thus inadequate constructions, a flexible flat band cable up to about 100 m in length is proposed, which can follow the settlement of the snow cover. A picture of the cable together with a sketch of the cross-section is shown in Fig. 16.5.

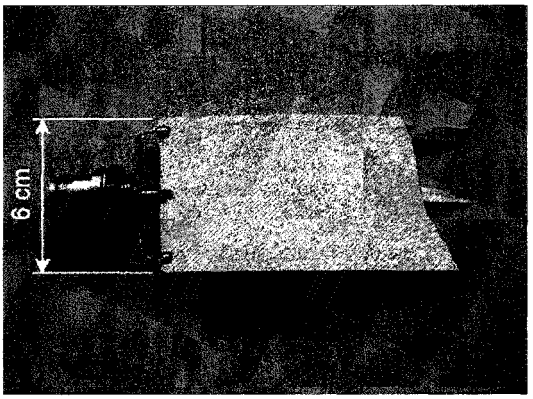

Fig. 16.5. The PE-insulated flat band cable (short section with uncovered conductor to show connection and geometry)

The electrical field concentrates around the conductors and defines a sensitive area of 3 to 5 cm around the cable. The spatial weighting of the measurements in the cross-section of the cable is directly related to the energy density distribution. The electric properties of the flat band cable used in this study can be calculated and measured. One can assume that the well-known equivalent circuit for the infinitesimal line section as shown in Fig. 16.6 fully describes the electrical properties of the line.

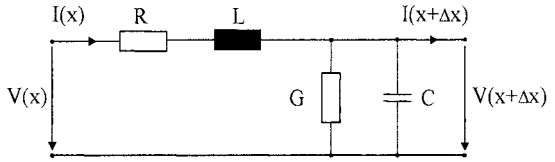

Fig. 16.6. Electric equivalent circuit of an infinitesimal section of a TEM transmission line

The white polyethylene (PE) insulation reduces heating due to solar radiation and the thin copper conductors have an advantageous low thermal capacity. Nevertheless, air gaps may develop around the flat band cable, e.g., due to multiple freezing and thawing cycles.

These air gaps cause under-prediction of the permittivity of the surrounding snow. To detect air gaps and correct the measurement results the three-wire cable is measured twice, both with small and with large spacing, leading to different measurement volumes as shown in Fig. 16.7. Thus an air gap has different effects on the volume and it is possible to correct it. A correction equation has been derived for calculating air gap size and true permittivity of snow [7].

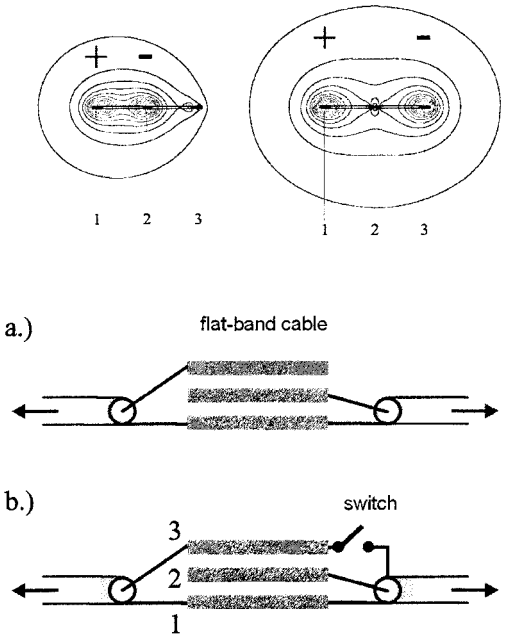

Fig. 16.7. Three-wire flat band cable: extension of the electromagnetic field for different connection possibilities. The cable is connected once from the left (a) and once from the right side (b)

16.5 Field Experiment Set-up

The new flat band cable sensor was tested at the high-elevation field site "Weissfluhjoch" at Davos (Switzerland) at 2550 m a.s.l. Fig. 16.8 shows an overview of this well-known avalanche test site which is equipped with numerous meteorological and nivological instruments and has a heated measurement shelter.

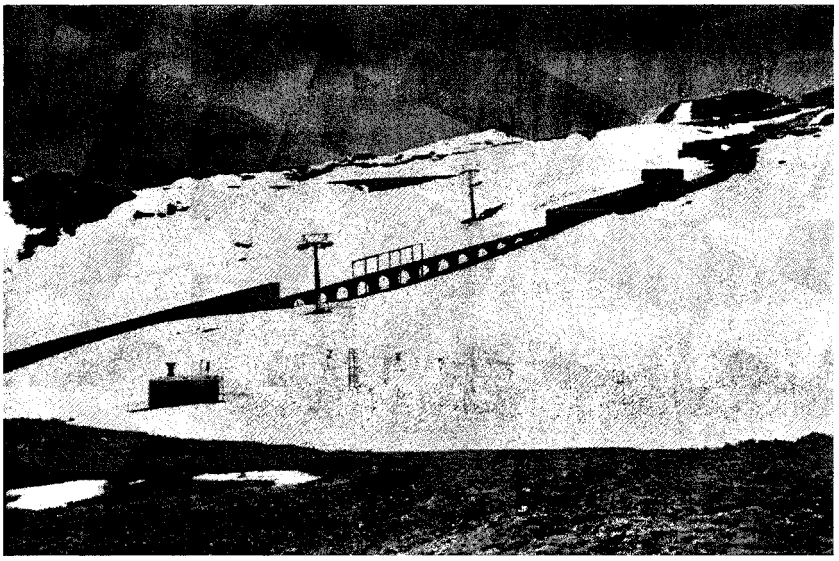

Fig. 16.8. Overview of the test-site at Davos with Parsenn cable car in the background

Two different set-ups were examined:

1. One cable was mounted sloping (Fig. 16.9) at an angle of 30° from the bottom to a mast with the aim of measuring the vertical properties of the snow pack (snow depth, density profile, snow water equivalent).
2. Three cables were placed horizontally on the snow surface at different stages of the winter in order to measure the spatial variability of the liquid water content and snow density, and especially to detect water conducting zones during the main snowmelt.

In the following only the evaluation of the horizontal cables is shown. These cables followed the natural settlement of the snow pack. The electronic measurement devices of the system were placed in the shelter approximately 10 m away from the cable sensors (Fig. 16.9). For the high-frequency measurements (100 MHz to 1 GHz) a TDR cable tester "Tektronix 1502B" was used the low-frequency measurements in the range of 1 kHz to 300 kHz were carried out with an impedance analyzer "HP-4192A". A PC and a home-made multiplexer completed the system. The measurements started on December 21, 2001 and ran automatically until the end of the winter season (June 21, 2002).

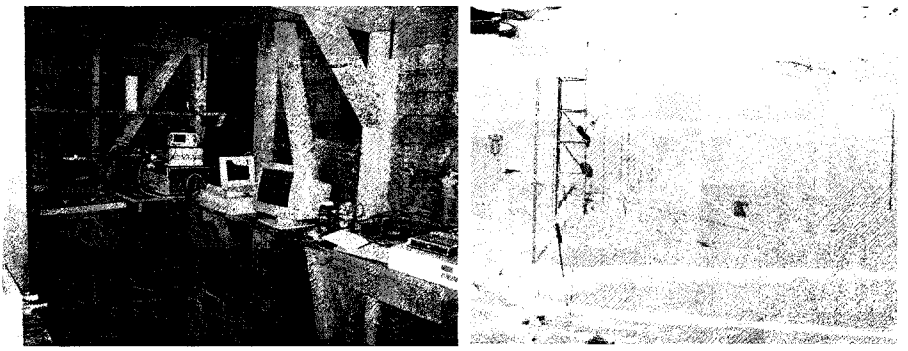

Fig. 16.9. The cable sensor system at "Weissfluhjoch", Davos (2550 m): the electronic devices in the shelter (*left*) and the test field with sloping cable sensor (*right*).

With the exception of some weeks in December, when an erroneous setting prevented the impedance analyzer from running, and in April, when the breakdown of an internal electronic component forced us to replace the impedance analyzer, the electronic system ran more or less failure-free throughout the entire winter season. The performance of the measurements and the position of the horizontal cables in the snow pack are shown in Fig. 16.10.

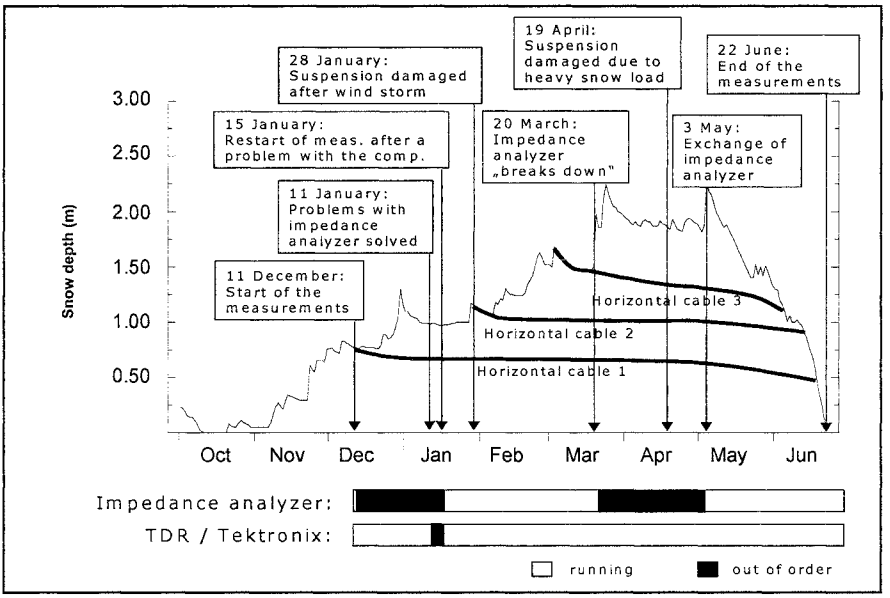

Fig. 16.10. Summary of the test measurements at Davos during winter 2001/2002 indicating problems and measures taken in the run over the season. Also, snow depth and position of the horizontal flat band cables are indicated

16.6 Experimental Results

The sloping flat band cable was able to withstand the harsh weather conditions quite well. However, with regard to the suspension and the supporting poles, which bent considerably when the snow load was heaviest, more sophisticated solutions need to be found. There were no clear indications of an air gap during the accumulation phase, but during melting an air gap was noticed at the sloping cable. The evaluation of the sloping cable is still under development, so only the results of the horizontal cables are shown.

The capacitance and dielectric permittivity of these cables for both the high- and low-frequency range were calculated from the raw signals. Figure 16.11 shows the capacitance in picofarads per meter of the lowest horizontal cable for both the small and large spacing measurement mode.

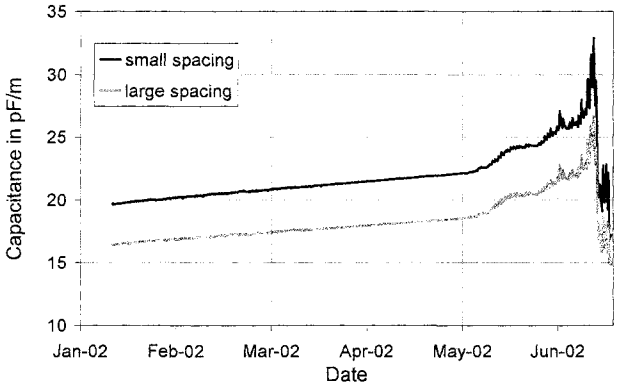

Fig. 16.11. Capacitance at high frequency of lowest horizontal cable

The clear difference between the two spacing modes is mainly caused by the different influence of the PEinsulation and is corrected by a calibration of the cable in well-defined materials.

Figure 16.12 shows the capacitance of the horizontal cable for the low-frequency measurements at 10 kHz. As expected the capacitance is much higher, thus leading to higher permittivity so that the differences in the water to ice permittivity ratio at the two frequencies is large enough to use the proposed evaluation method.

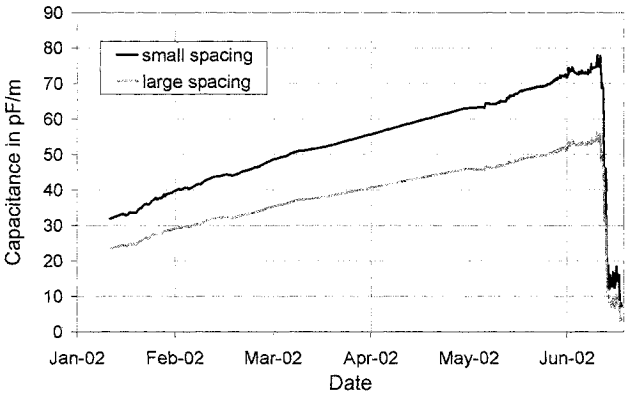

Fig. 16.12. Capacitance at low frequency (10 kHz) at lowest horizontal cable

The calculated high-frequency permittivity is shown in Fig. 16.13. It can be seen that the calibration was successful and the small and large spacing modes nearly yield identical results. We did not find any evidence for significant voids around the horizontal cables when we excavated dummy flat band cables, so the presence of air gaps around the horizontal cables can be excluded.

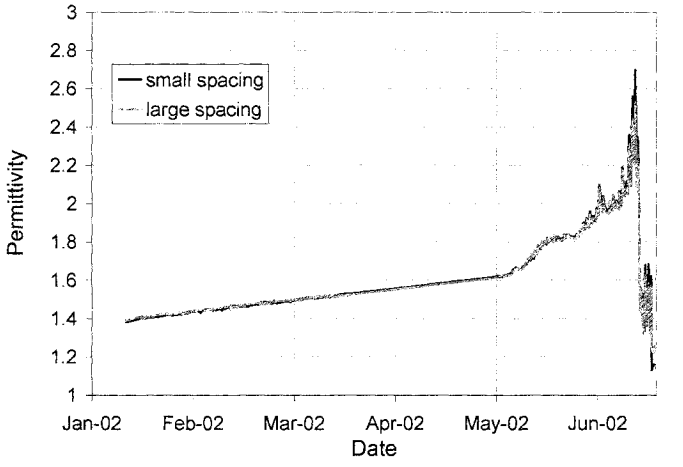

Fig. 16.13. High-frequency permittivity at lowest horizontal cable

From the curve it can be seen that the measurements started at the end of January 2002 and the cable was successively covered with snow. The slight increase in permittivity is caused by the increase in density of the dry snow pack. At the beginning of May, the sharp rise of the curve indicates the start of the melting period, where liquid water penetrates the snow pack. Although interrupted by a short cold period at the end of May when the capacitance stayed constant for

a few days, the melting intensified in June. In this state also, variations in permittivity between day and night times due to melting and refreezing processes are clearly visible. At the end of June, the sharp drop in permittivity is caused by the melt-out of the cable and its exposure to air. The determined dimensions of the high-frequency permittivity are in the same order of magnitude as that found by Tiuri et al [8] for similar snow packs.

The low-frequency permittivity (at 10 kHz) is given in Fig. 16.14. It is approximately five times higher than the high-frequency permittivity and thus gives the possibility to use the equations above to determine the density and the liquid water content of the snow pack. The steeper increase of the curve in the dry snow phase compared to the high-frequency results is due to the much higher permittivity of ice at the low frequency (ε_{ice}(10 kHz) = 38.11) used, which influences the permittivity of the ice–air mixture. For the same reason, the variations during the melting phase are less pronounced. The bigger difference between the small and large spacing modes for the low-frequency permittivity is still a question of adequate calibration in the low-frequency range and will be improved in future.

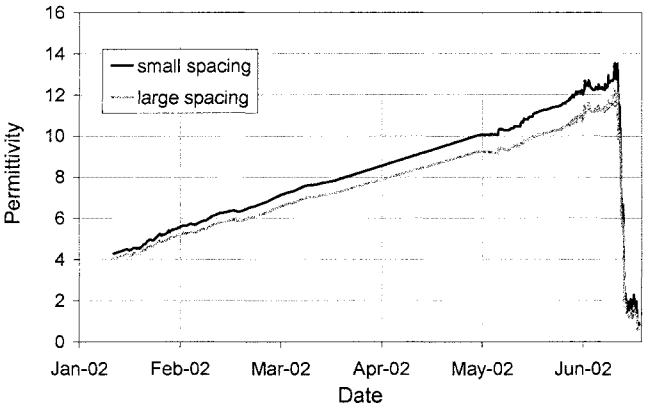

Fig. 16.14. Low-frequency permittivity at lowest horizontal cable

The combination of high- and low-frequency permittivity measurements finally led to the liquid water content along the horizontal cable shown in Fig. 16.15. Practically no liquid water was detected with the horizontal cable until the end of April, when the snow pack had reached its maximum height. This is supported by the snow temperature measurements taken at the same height as the cable (Fig. 16.16), which indicate dry snow conditions due to temperatures well below zero before this period. If the small amounts of 0.1 to 0.2% water content that were measured during the dry snow phase are realistic and possible is still a topic of the current discussion and remains unclear at the moment.

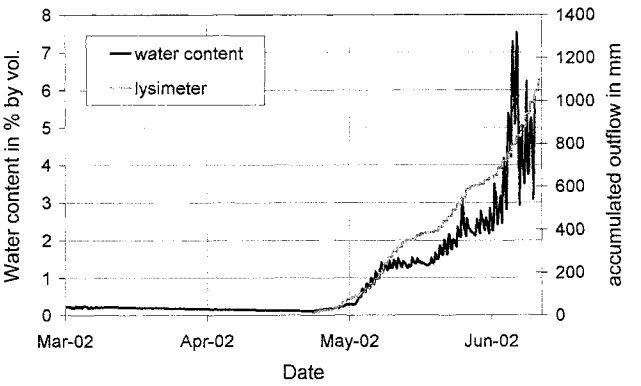

Fig. 16.15. Calculated liquid water content at lowest horizontal cable compared to accumulated outflow of lysimeter

Once the snowmelt set in at the end of April, a steadily increasing liquid water content was measured with the horizontal cable, indicating the downward penetration of the wetting front. The cable even reacted remarkably to the diurnal variation by detecting slightly higher water contents (0,1%-0,5%) during the day when melting occurs and lower water contents during the night, when the liquid water refreezes again due to lower temperatures.

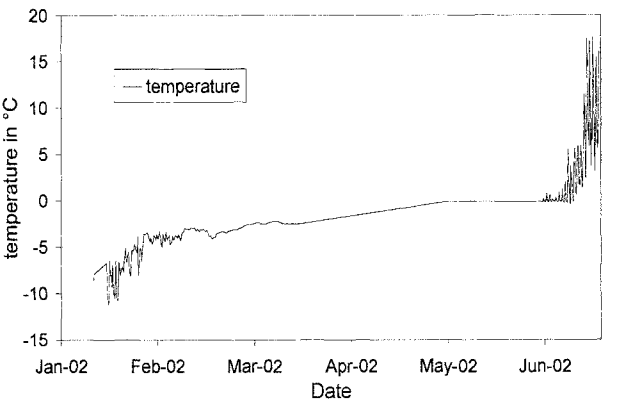

Fig. 16.16. Temperature of snow pack at same height than horizontal cable during winter

Figure 16.16 shows the temperature of the snow pack during winter at the same height as the cable. The part of the dry snow pack with temperatures below 0°C and the wet snow pack with temperatures of 0°C and above can be clearly distinguished and corresponds to the results found with the capacitance and permittivity measurements. It can also be seen that the snow temperature sensor is

no longer covered with snow in the middle of June and is thus influenced by air temperature. This corresponds also with results of the horizontal cable, which melted out in the middle of June. The slight difference is caused by the settlement of the cable, being covered by snow a little longer than the temperature sensor, which is mounted on the ground like a candle and thus cannot settle with the snow cover.

The natural settling of the snow cover was reflected nicely in the horizontal cable measurements. The snow density (Fig. 16.17) increased from initially 200 kg/m^3 to approximately 450 kg/m^3 at the end of the winter season, which was in accordance with manual snow density measurements of the corresponding snow layers taken in the field every fortnight. We have no explanation for the high manual values at the beginning of the measurement period. The other horizontal cables located at different depths of the snow pack also correctly reproduced a lower density in the upper part of the profile and a faster compaction during the snowmelt.

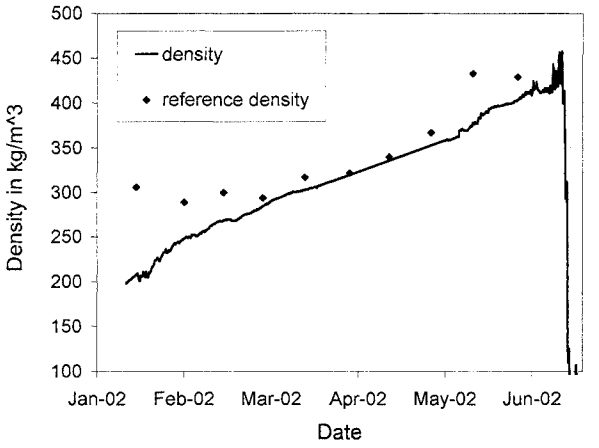

Fig. 16.17. Density of snow pack during winter 2002 at horizontal cable 2

With the TDR signal reconstruction algorithm developed by Schlaeger [9], the distribution of liquid water content along one of the horizontal cables was also reconstructed for two different stages during the melting period in May.

With regard to the spatial variation of liquid water, the horizontal flat band cable nicely demonstrated the formation of preferential water flow paths (Fig. 16.18), which is the natural process of water transport in a melting snow pack [10]. The horizontal cable at about 1 m below the snow surface indicated an emerging water conducting zone in mid May at 14 m from the beginning of the cable, as well as a newly developing flow finger at 8 m. These results will open up new possibilities for snow hydrology research and especially for the forecast of wet snow avalanches.

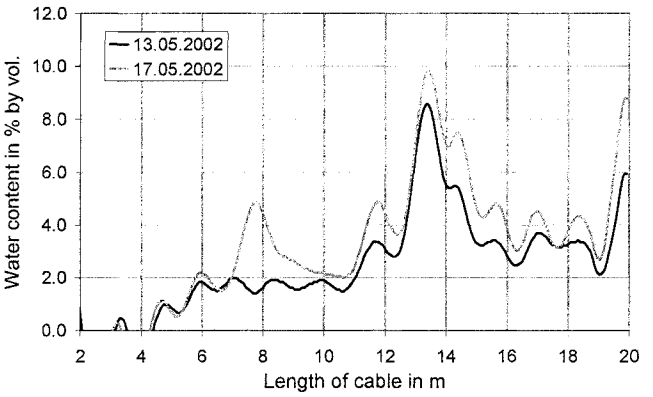

Fig. 16.18. Spatial variation of liquid water content along the upper horizontal cable at two days during the melting period

Following these promising results, a second field test of the new flat band cable has been started at Davos and will go on throughout winter 2002/2003.

16.7 Conclusion

It has been demonstrated that dielectric methods are very well suited for snow moisture determination. A combination of high- and low-frequency measurements gives a good opportunity of determining both the liquid water content and the density of the snow pack.

The measurement results yielded good correspondence of the snow pack density with manual reference measurements taken twice a month at the measurement site. Also, the determination of liquid water content from measurements of high- and low-frequency dielectric permittivity gave plausible results both compared to lysimeter data taken on the test field and with regard to the spatial variation of flow fingers that are normally experienced in a natural snow pack.

In light of these first results, the sensors seem to have the promise to become operational tools for continuous and large-scale monitoring of snow cover properties. The devices' suitability for the measurements has been demonstrated, but there is a dire need for an improvement of the instrumentation set-up to withstand the harsh conditions of Alpine winter seasons. This will be a task for the future.

Acknowledgments

Parts of this work have been carried out within the EUproject SNOWPOWER (5th framework, NNE5/2000/251).

References

1. Stein J, Gaetan L, Levesque D (1997) Monitoring the dry density and the liquid water content of snow using time domain reflectometry. Cold Regions Science and Technology 25:123-136
2. Maetzler C (1996) Microwave permittivity of dry snow. IEEE Trans Geosc Remote Sens 34:573-581
3. Denoth A (1994) The monopole antenna: A practical snow and soil wetness sensor. IEEE Trans Geosci Remote Sens 35:1371-1375
4. Denoth A (1989) Snow dielectric measurements. Adv Space Res 9 (1):233-243
5. Ulaby FT, Moore RK, Fung AK (1986) Microwave dielectric properties of natural earth materials. In: Ulaby FT, Moore RK, Fung AK (eds) Microwave remote sensing, vol III, From theory to applications. Artech House, Norwood, MA, pp 2017-2027
6. Looyenga H (1965) Dielectric constant of heterogeneous mixtures. Physica 31:401-406
7. Huebner C (1999) Entwicklung hochfrequenter Messverfahren zur Boden- und Schneefeuchtemessung. Wiss Ber FZKA 6329, Forschungszentrum Karlsruhe
8. Tiuri M E, Sihvola AH, Nyfors EG, Hallikainen MT (1984) The complex dielectric constant of snow at microwave frequencies. IEEE J Ocean Eng 9(5):377-382
9. Schlaeger S (2002) Inversion von TDR-Messungen zur Rekonstruktion räumlich verteilter bodenphysikalischer Parameter. Veröffentlichungen des Instituts für Boden- und Felsmechanik, vol 156, Karlsruhe
10. Marsh P, Woo M-K (1984) Wetting front advance and freezing of meltwater within a snow cover: 1. Observations in the Canadian Arctic. Water Resour Res 20(12):1853-1864